Heliyon 10 (2024) e23955

Contents lists available at ScienceDirect

Heliyon

journal homepage: www.cell.com/heliyon

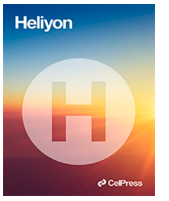

Antibacterial and osteoinductive properties of wollastonite scaffolds impregnated with propolis produced by additive manufacturing

Ana Isabel Moreno Florez [a], Sarita Malagon [b], Sebastian Ocampo [a], Sara Leal-Marin [c], Jesús Humberto Gil González [d], Andres Diaz-Cano [a], Alex Lopera [e], Carlos Paucar [a], Alex Ossa [f], Birgit Glasmacher [c], Alejandro Peláez-Vargas [b], Claudia Garcia [a,*]

[a] *Grupo de Cerámicos y Vítreos, Universidad Nacional de Colombia sede Medellín, Medellín 050034, Colombia*
[b] *Faculty of Dentistry, Universidad Cooperativa de Colombia sede Medellín, Medellín 055422, Colombia*
[c] *Institute for Multiphase Processes (IMP), Leibniz University Hannover, Garbsen, Germany, Lower Saxony Center for Biomedical Engineering, Implant Research and Development, Hannover, Germany*
[d] *Departamento de ingeniería agrícola y alimentos. Facultad de ciencias agrarias. Universidad Nacional de Colombia sede Medellín, Colombia*
[e] *Grupo de Nanoestructuras y Física Aplicada (NANOUPAR), Universidad Nacional de Colombia, La Paz 202017, Colombia*
[f] *School of Applied Sciences and Engineering, Universidad Eafit, Medellín 050022, Colombia*

A R T I C L E I N F O

Keywords:
Scaffolds
Propolis
3D printing
Antibacterial activity
Cell proliferation

A B S T R A C T

Biocompatible ceramic scaffolds offer a promising approach to address the challenges in bone reconstruction. Wollastonite, well-known for its exceptional biocompatibility, has attracted significant attention in orthopedics and craniofacial fields. However, the antimicrobial properties of wollastonite have contradictory findings, necessitating further research to enhance its antibacterial characteristics. This study aimed to explore a new approach to improve *in vitro* biological response in terms of antimicrobial activity and cell proliferation by taking advantage of additive manufacturing for the development of scaffolds with complex geometries by 3D printing using propolis-modified wollastonite. The scaffolds were designed with a TPMS (Triply Periodic Minimal Surface) gyroid geometric shape and 3D printed prior to impregnation with propolis extract. The paste formulation was characterized by rheometric measurements, and the presence of propolis was confirmed by FTIR spectroscopy. The scaffolds were comprehensively assessed for their mechanical strength. The biological characterization involved evaluating the antimicrobial effects against *Staphylococcus aureus* and *Staphylococcus epidermidis*, employing Minimum Inhibitory Concentration (MIC), Zone of Inhibition (ZOI), and biofilm formation assays. Additionally, SaOs-2 cultures were used to study cell proliferation (Alamar blue assay), and potential osteogenic was tested (von Kossa, Alizarin Red, and ALP stainings) at different time points. Propolis impregnation did not compromise the mechanical properties of the scaffolds, which exhibited values comparable to human trabecular bone. Propolis incorporation conferred antibacterial activity against both *Staphylococcus aureus* and *Staphylococcus epidermidis*. The implementation of TPMS gyroid geometry in the scaffold design demonstrated favorable cell proliferation with increased metabolic activity and osteogenic potential after 21 days of cell cultures.

* Corresponding author. Universidad Nacional de Colombia. Carrera 65 No 59A-100 Medellin, Colombia.
E-mail address: cpgarcia@unal.edu.co (C. Garcia).

https://doi.org/10.1016/j.heliyon.2023.e23955
Received 18 August 2023; Received in revised form 30 November 2023; Accepted 18 December 2023
Available online 18 December 2023

1. Introduction

Systematic reviews about different bone regeneration techniques have been frequently reported in the last five years, and recurrent conclusions are found. The design of randomized clinical trials to study bone healing, stability, complications, aesthetics, cost, and surgical time of bone graft procedures is required [1]. Several diseases related to bone tissue affect the quality of life in patients around the globe [2]. Bone from the iliac crests, ribs, or flat bones from the skull may be used for congenital defects, such as craniosynostosis and cleft palate, as well as defects associated with trauma, tumors, and other pathologies [3]. However, the highest limitations of bone grafting for craniofacial areas are the availability of bone tissue for autograft and the morbidity of surgical procedures during bone harvesting. Orthopedic, neurosurgery, plastic surgery, and dentistry conduct more than 2.2 million procedures for bone reconstructions per year [4]. Although such treatment approaches are safe and predictable, failure rates have been reported to range between 1.5 and 20 % [5] mainly caused by bacterial osteomyelitis during the post-surgical stage. These failures might increase due to drug resistance to superbug spreading in hospitals [6], but natural products might provide new tools to fight these microorganisms [7].

Bone regeneration is a complex process in which biological aspects, such as bacteria/cell homeostasis and osteogenesis, innervation, and angiogenesis, and physical features (architecture and mechanical properties) from macro and nanoscale need to be considered. Several 2D and 3D technologies have been developed to provide new approaches to improve bone repair. However, in the pathway from bench to clinical use, several technologies have not crossed the stages of *in vitro* studies, since many questions remain to be answered, including scalability, massive sterilization, and quality control of products derived from these current technologies. Another restriction for these technologies to mature has been one that is inherent to the public health system: a systematic review that evaluated 158 studies found an imbalance in the technical set-up between public hospitals and private hospitals/companies to simulate and fabricate customized 3D bone grafts for complex patients. They also found that the main challenges are related to time, equipment cost, and lab-technician skills [8].

Bone regeneration is a size-defect-dependent process ranging from self-repairing (<4 mm) to critical-sized bone defects that are not repaired naturally or are repaired by different tissues. Open alveoli derived from exodontia, gunshot trauma, or congenital defects need different bone graft volumes [9]. Open alveoli might be filled using lyophilized bone particles or calcium/phosphate synthetic powders. However, other defects, exhibiting complex shapes, have been treated using membranes or metallic mesh to maintain the bone particles confined. However, these approaches present several complications during surgery.

CAD/CAM based on subtractive techniques allows the building of customized bone grafts using polymer, metallic (titanium alloys), and ceramic materials (zirconia, alumina, feldspathic porcelain) that exhibit limited biological functionality [10]. Similarly, 3D-engineered scaffolds combining polymer, metallic, or ceramic materials to module or carry cells, drugs, or molecules have been developed. Their mechanical features include a 2–50 MPa compressive strength 11–13] and porous size between 300 and 1200 μm [14]. Several techniques have been used to manufacture these scaffolds, including replica molding, sacrificial layers, ice molding, and salt leaching [15]. Currently, 3D printing and combined methods, including 3D printing and electrospinning, have been developed to combine the micro and nano scales, but they remain *in vitro* approaches. However, FDM techniques, stereolithography, selective fusion by electron beam, and ceramic sintering have been reported for maxillofacial clinical applications [16]. 3D direct printing of bioceramic slurries shows advantages, such as lower costs and improved mechanical properties. This technique assists in obtaining multiscale porosity which is properly distributed and located to favor osteogenesis and neovascularization. However, its main disadvantage is related to low efficiency [16,17].

Wollastonite ($CaSiO_3$) is a mineral that exhibits high *in vitro* reactivity to produce hydroxyapatite on surfaces [18], increase cellular viability, and promote differentiation of the osteoblast lineage [19]. Its mechanical properties are similar to cortical bone [20,21]. However, pure wollastonite produced by sol-gel methods has shown poor antibacterial activity [22,23]. Several modifications of wollastonite have been described to promote antibacterial properties, such as silver, copper, and titania doping. However, their clinical applications are not reported [24,25]. Other strategies have been used to produce functionalized scaffolds loaded with antimicrobial drugs, including minocycline, vancomycin, penicillin, and streptomycin [26]. However, to the best of our knowledge, these drugs have been used to coat bioceramics and bioglass scaffolds, and although antibacterial properties were found, a controversy is maintained about whether these types of functionalization contribute to the increase in the production of super-resistant strains. Currently, natural antimicrobial products, such as oregano, garlic, turmeric, and propolis avoid such risks due to their composition, which includes phenols, quinines, saponins, flavonoids, tannins, coumarins, terpenoids and alkaloids [27]. Propolis has been reported as non-inflammatory [28], a protector of nervous fibers, tissues, and apoptotic processes. It is also antioxidant and antimicrobial [29–38]. In this context, wollastonite scaffolds impregnated with propolis might control bacterial growth in the initial stages of bone healing and might prevent the occurrence of superbug strains, thus contributing to enhanced bone repair.

The purpose of this work was to fabricate antibacterial and biocompatible propolis-modified wollastonite 3D-printed scaffolds to improve the *in vitro* biological response in terms of antimicrobial behavior and cell proliferation. In this way, the scaffolds produced are enhanced as tools for bone regeneration.

2. Materials and methods

2.1. Ceramic slurry preparation

The ceramic paste is composed of commercial wollastonite powder (NYAD® M1250) with a particle size of 4 μm and acicular morphology, Polyvinyl alcohol (PVA, Sigma, 98 % hidrolyzed, USA), Carboxymethyl cellulose (CMC, Sigma, USA), and deionized

water. The formulation of the ceramic paste was obtained through the application of a fractional factorial design of experiments, in which each component of the mixture was taken as an input variable, and the required force to extrude the suspension into a syringe was studied as a response variable. The experiment was conducted by applying normal force using a universal testing machine (Instron 3366 Universal Testing System) with a 500 N load cell, thus simulating the printing process. The proportions ultimately used for printing with the prepared ceramic paste were Wollastonite 59.97%w/w, CMC 0.03%w/w, deionized water 37.75%w/w, and PVA aqueous solution 2.25%w/w.

A 5 % v/v aqueous solution of polyvinyl alcohol (PVA) was prepared. Separately, CMC was added at 0.01 wt% to the dry wollastonite powder in a beaker. The premixtures were homogenized. The PVA aqueous solution was added to the powder mixture. The mass of the powder was 1.5 times the mass of the PVA aqueous mixture. The suspensions were manually mixed with a spatula and then a Heidolph DIAX 900 homogenizer was used at a speed of 8000 rpm for 4 min to homogenize the suspension. Subsequently, the suspensions were refrigerated at 4 °C for 24 h. The suspensions were mixed again before printing. This ensures a homogeneous and smooth flow of the suspension during printing.

2.2. Rheological behavior

The rheological behavior of the suspensions was evaluated using an automatic dynamic shear rheometer (RHEOTEST® medingen GmbH 81-PV6202). A 36 mm diameter plate configuration (P1) with a 0.5 mm gap was used. A range of shear rates from 0.01 to 100 s-1 was evaluated, and shear stresses were measured.

2.3. 3D printing

The scaffolds were printed using a 3D printer (Delta WASP 2040). The G-code used to print the scaffolds was generated using Cura software (Ultimaker, Netherlands). A *.STL file was used to define the volume of the sample. It was then sliced using the Gyroid infill pattern, without outer walls. The parameters used for the printing process are listed in Table 1.

A custom-made printer head was used to hold a 5 ml syringe with an 18-gauge needle. A microscope slide was used as the printing substrate. The scaffolds were printed using a triple periodic minimal surface (TPMS) infill pattern [39]. Two different scaffold geometries were printed: cylindrical (⌀ = 10 mm and h = 5 mm), and cubic (w = 16 mm, l = 16 mm and h = 10 mm) which were used for biological and mechanical characterization, respectively. Scaffolds were printed and air-dried for 24 h.

The scaffolds were printed and air-dried for 24 h. Then, the scaffolds were subjected to a heat treatment in a Sentro Tech SX1700 oven using the following curve: from room temperature to 200 °C with a heating rate of 2 °C/min, this temperature was maintained for 1 h. Then, the temperature was increased to 500 °C at 2 °C/min, and this temperature was maintained for 3 h to remove organic residues. In the final phase of the heat treatment, aimed at sintering, the scaffolds were exposed to a temperature of 1180 °C for 3 h [40]. This temperature was reached at a rate of 2 °C/min. After the heat treatment, the samples were allowed to cool naturally.

2.4. Porosity and pore interconnectivity

To measure the porosity and pore interconnectivity of the scaffolds, the ASTM C373-88 standard [41] and the method described by Liu et al. [42] were used. The apparent density of the scaffold (ρ_b) is calculated using equation (1).

$$\rho_b = W_D / W_S - W_U \quad (1)$$

Where W_D is the weight of the dry scaffolds, W_U is the weight of the immersed scaffolds, and W_S is the weight of the saturated scaffolds.

Then the total porosity of the scaffold (φ_t) was calculated using equation (2) to determine the water absorption capacity of the scaffold.

$$\varphi_t = W_S - W_D \; / \; W_D \; x \; 100 \quad (2)$$

Table 1
Printing and infill parameters.

Parameter	Value
Layer Height	0.7 mm
Initial Layer Height	0.4 mm
Line width	0.3 mm
Wall line count	0
Top/Bottom thickness	0.0 mm
Infill density	10 %
Infill line distance	1.5 mm
Infill pattern	Gyroid
Infill overlap percentage	5.0 %
Infill overlap	0.015 mm
Flow	20 %
Print speed	3.0 mm/s
Travel speed	40 mm/s

$$\varphi_a = (W_S - W_D \ / \ \rho_a \text{ x } V) \text{ x } 100 \quad 3$$

$$P_i = (\phi_a \ / \ \phi_t) \quad 4$$

To obtain a measure of the interconnectivity between the pores, it was necessary to calculate the open porosity (φ_a) using equation (3). Lastly, the percentage of interconnected pores (P_i) was calculated using equation (4). ρ_a corresponds to the theoretical density of water, and ρ_r is the real density of the scaffold. To obtain the real density (ρ_r) of the scaffold, the pycnometer method was employed [43]. For this purpose, a scaffold was pulverized, and the weight of a clean and dry pycnometer (M_1), was measured. Then, the pycnometer was filled with distilled water until the meniscus, and its mass (M_2), was obtained. Next, the pycnometer was emptied to half of its volume, and the weight (M_3), was measured. Subsequently, the pulverized scaffold was added to the pycnometer, and the weight (M_4) was determined. Finally, the pycnometer was filled again with distilled water, ensuring the elimination of air bubbles and avoiding their formation. The weight after filling was measured as (M_5). The mass of the scaffold was calculated as ($M_4 - M_3$), and its volume is the volume of the displaced liquid.

2.5. Propolis samples and Extraction

The propolis samples were obtained from beehives located in the Araucanian foothills, Colombia, and were supplied by beekeepers from Tame (Colombia). Once collected, the propolis samples were stored at 4 °C. Ethanol extracts of propolis were prepared by mixing 10 g of each propolis sample with 100 mL of 70 % v/v ethanol. It was kept under agitation for 48 h at a controlled speed of 120 rpm at 37 °C and then subjected to a gravity filtration process. A rotary evaporator (RE-20000E) at 40 °C and 2.5 Bar was used to remove the solvent and obtain clarified propolis extracts.

2.6. Scaffold impregnation procedures

For the impregnation of the scaffolds, 20 μL of ethanolic propolis extract was added to the surface of each scaffold. They were placed in a positive pressure chamber (Wiropress, BEGO) for 3 min. Once it was confirmed that the extract had been absorbed, the process was repeated until the total absorbed volume reached 150 μL.

2.7. FTIR

For Fourier Transform Infrared (FT-IR) analysis, the propolis extracts, sintered wollastonite, and propolis-impregnated wollastonite were evaluated using a spectrometer (Spectrum 2, PerkinElmer) with an attenuated total reflectance accessory. At least 3 spectra were obtained from different areas in each sample (each spectrum represents the average of 100 scans between 400 cm^{-1} and 4000 cm-1 with a resolution of 4 cm^{-1}). Subsequently, baseline correction and the average spectrum were calculated using numerical software (Matlab, Mathworks, Mass).

2.8. Biological characterization

The antibacterial activity was evaluated against the standard strains *Staphylococcus aureus* (ATCC 25175) and *Staphylococcus epidermidis* (ATCC 12228) following the procedure described by the Clinical and Laboratory Standards Institute (CLSI). The strains were previously inoculated onto Petri dishes containing Mueller Hinton agar (Merck, Germany) and incubated at 37 °C for 24 h. To obtain bacterial inocula, the strains were cultured to the exponential phase in Brain Heart Infusion medium (Merck, Germany) at 37 °C for 24 h and adjusted by diluting fresh cultures to achieve turbidity equivalent to 90 NTU (approximately 1.5×10^8 CFU/mL).

To determine the MIC, the broth microdilution assay was performed in 96-well microplates. A volume of 100 μL of Mueller Hinton broth (Merck, USA) and 100 μL per well of the propolis ethanolic extract (EEP) were added, following the procedure described by the CLSI with some modifications [44]. A stock solution of 100 mg/mL of EEP was prepared and then diluted in Mueller Hinton broth using serial dilutions (in a 1:2, v/v ratio) at concentrations ranging from 50 to 2000 μg/mL in the microplates. Approximately 50 μL of bacterial suspension, with an approximate concentration of 1.5×10^6 CFU/mL, was added to the wells containing 100 μL of Mueller Hinton broth with different final concentrations of EEP. The results were observed after adding 50 μL of resazurin solution (100 μg/mL) and incubating again at 37 °C for 2 h. Blue staining in the microplates indicated the absence of bacterial growth for *S. aureus* and *S. epidermidis*, while pink staining indicated bacterial growth. Dilutions with 70 % v/v ethanol (solvent of the extracts) in Mueller Hinton broth were performed to assess the ethanol's impact, and Mueller Hinton broth was used as the negative control. The MIC values were defined as the concentration that inhibited bacterial growth. This assay was performed in triplicate.

The disk diffusion method was used to evaluate the antibacterial activity. Twenty milliliters of Mueller-Hinton agar medium were poured into Petri dishes. Each Petri dish was inoculated with the bacterial inoculum (approximately 1.5×10^8 CFU/mL). Subsequently, the scaffolds impregnated with propolis extracts (IS) and without propolis extracts (US) were placed. Chlorhexidine and PBS were used as positive and negative controls, respectively. After 24 h of incubation at 37 °C, the zone of inhibition was measured in mm using Image J software. Each experiment was performed in triplicate.

For biofilm formation inhibition tests an inoculum of 90 NTU (approximately 1.5×10^8 CFU/mL) was prepared, and two serial dilutions at a 1:10 ratio were performed to obtain a concentration of 1.5×10^6 CFU/mL for each strain. Sterilized scaffolds were divided into a) the first group consisted of propolis-impregnated scaffolds (IS), and b) the second group consisted of untreated scaffolds

(US). Each group was inoculated with 1 mL of the respective strain's inoculum. The scaffolds were incubated for 24 h and 48 h at 37 °C and 5 % CO_2. After the incubation period, 3-(4,5-dimethyl-2-thiazolyl)-2,5-diphenyl-2H-tetrazolium bromide (MTT, Merck, Germany) was added, and the scaffolds were further incubated for 2 h at 37 °C and 5 % CO_2. The MTT solution was then removed, and dimethyl sulfoxide (DMSO, Sigma, USA) was added. Absorbance at 550 nm was measured using a spectrophotometer (Zeiss, Germany).

Human osteosarcoma cells (SaOS-2) provided by Dr. Yvonne Roger from Clinic for Orthopedics at Hannover Medical School were used, they are isolated cells from human osteosarcoma (connective and supportive tissues). The cells were seeded in high-glucose DMEM medium (Roth, Germany) supplemented with 10 % heat-inactivated fetal bovine serum (FBS) (Bio&sell, Germany) and 1 % penicillin-streptomycin at 37 °C and 5 % CO_2, for the first 7 days. The medium was changed every 24h. Subsequently, the cells were exposed to a differentiation medium adding 5 mM β-glycerophosphate (Merck, Germany), 50 mM ascorbic acid (Merck, Germany), and 10 nM dexamethasone (Merck, Germany) for 28 days.

For cell cultures, sterile scaffolds were taken and immersed in PBS (Merck, Germany) for 72 h to prevent an initial burst release of calcium ions that could potentially damage the cells. Scaffolds were impregnated with 150 of propolis (IS) and the control group were untreated scaffolds (US).

For the cell proliferation assay 5×10^4 cells/cm^2 of SaOS-2 were seeded onto IS and US in a 24-well plate (TPP, Switzerland) and cultured for 28 days in the previously described medium. Cell viability measurements were taken at 1, 3, 7, 14, 21, and 28 days. Cell viability was determined using a resazurin reduction method [45]. A working solution of 44 μM Alamar Blue Reagent was prepared in a preheated culture medium immediately before the experiments, and 1 ml was added to the samples. The cultures were incubated for 1.5 h with the Alamar Blue reagent, and fluorescence measurements were quantified using a fluorescence reader (Tecan Infinite M200 Nanoquant, USA) with an excitation wavelength of 570 nm and an emission wavelength of 600 nm. A calibration curve of cell number and fluorescence measurement was constructed ($r^2 = 0.98$). Additionally, the assay was performed in 24-well plates and cultured under the same conditions as the scaffolds to obtain a control measurement. The results are expressed as the percentage of viability found on the scaffolds relative to control samples. The assays were performed in triplicate.

To evaluate the morphology of cell adherence, the scaffolds were observed using a scanning electron microscope (SEM, S3400 N, Hitachi, Japan) obtaining images with secondary electrons (SE) and backscattered electrons (BE) using a working distance of 30 mm and an acceleration voltage of 20 kV. The scaffolds were prepared by washing with 0.1 M cacodylate buffer (Merck, Germany) and then fixed with 3 % glutaraldehyde (Merck, Germany) for 10 min. They were subsequently washed with PBS (Merck, Germany) and dehydrated using sequential ethanol solutions (from 25 to 99 % v/v). After overnight drying, a 35 nm layer of Au–Pd was coated onto the samples using a Minisputter SC7620 (Quorum Technologies, UK).

A qualitative approach to the osteogenic process was performed using histochemical staining, presence in the extracellular matrix of calcium (von Kossa assay and Alizarin Red), and Alkaline Phosphatase (ALP assay) was conducted. Initially, SaOS-2 cells were seeded (5×10^4 cells/cm^2) onto IS and US scaffolds in a 24-well plate (TPP, Switzerland) and cultured for 7 days in the aforementioned medium. On day 7, the cells were cultured with a differentiation medium, and staining measurements were taken at 21 and 28 days. Additionally, cells were seeded in 24-well plates without scaffolds to observe the morphology and behavior of the cell line without scaffold interaction. The cells were fixed to the scaffolds with 3 % glutaraldehyde (Merck, Germany) for 15 min and then washed with PBS (Merck, Germany).

For von Kossa staining, scaffolds were treated with a 1 % silver nitrate solution (Merck, Germany) and exposed to UV light for 1 h. They were then washed with distilled water and covered with a 5 % sodium thiosulfate solution (Merck, Germany) for 3 min. After a wash with distilled water, the scaffolds were left to dry [46]. For Alizarin Red staining, scaffolds were treated with sterile 4 nM Alizarin Red (Merck, Germany) solution for 2 min, washed with deionized water, and then 10 mM HCl in 70 % ethanol was applied for 15 s. The scaffolds were left to dry. For the ALP staining, the Na–naphthyl phosphate (Merck, Germany) solution was added with Tris buffer (Sigma, USA) and stirred for 10 min. Then, fast blue (Sigma, USA) was added and kept stirring for 5 min. The staining solution was added and kept in the dark for 1 h, followed by a wash with PBS and allowed to dry [46]. Finally, the scaffolds were observed using light microscopy (Zeiss Stemi DV4) [46]. Staining on scaffolds without cells was used as a control measure for staining on the material. The experiments were conducted in triplicate.

2.9. Mechanical test

The mechanical response of the samples was measured by monotonic compression at a rate of 0.5 mm/min using a UTS (Instron 3366, Instron, MA, EE.UU.) equipped with a 10 kN load cell. The compressive load and displacement were recorded during the tests and the maximum load or failure load of each test was used to calculate the maximum stress supported by the samples as a measure of the compressive strength of each scaffold. The measurements were taken at time 0, which describes the scaffolds before being subjected to cell culture. Additionally, measurements were taken after 21 and 28 days of cell culture to get an estimation of the effect of cell adherence on the mechanical response of the scaffolds.

2.10. Statistical analysis

All experiments were performed in triplicate. The results were expressed as mean ± standard deviation (SD). Statistical analysis was conducted using SPSS Statistics software (V21, IBM, USA). An unpaired Student's t-test was used to assess the significance between experimental groups. A p-value $\measuredangle$ 0.05 was considered statistically significant.

3. Results and discussion

3.1. Characterization of the scaffolds

The formulated ceramic paste allowed for the printing of cylindrical scaffolds with a TPMS gyroid geometry, measuring 5 mm in height and 5 mm in radius, with an average pore size of 780 μm. Fig. 1a-c and Fig. 1i,j) shows the sinusoidal shape of the obtained layers. Each printed layer measures approximately 500 μm. SEM photomicrographs of the wollastonite particles (Fig. 1 (d,e)) revealed the characteristic prismatic crystal structure of this mineral. Elemental Energy-Dispersive X-ray Spectroscopy (EDS) characterization of the scaffold obtained by 3D printing, showed the presence of Si, Ca, and O (Fig. 1(f–h)). In Fig. 1(k and l) macrophotographs of the scaffolds after being impregnated with propolis can be seen. The scaffolds geometry is not compromised by the impregnation of the propolis.

The porosity and interconnectivity tests showed a total porosity of 50 ± 4 %, an open porosity of 59 ± 4 %, and a pore interconnectivity percentage of 84 ± 1 %. High porosities are desired in the design of scaffolds for bone regeneration as they facilitate cell proliferation processes [47]. The percentages of porosity present in natural bone tissue vary depending on the type of bone [48]. In the case of trabecular bone, a total porosity between 30 % and 90 % has been reported. Specifically, for mandibular trabecular bone, the total porosity ranges between 70 % and 90 %, while in cortical bone, it is found between 5 % and 30 %. Given the reported results, the scaffold designed in this study has potential applications in the repair of trabecular bone tissue. Pore sizes larger than 300 μm enable the adhesion, migration, and proliferation of osteoblasts through the activation pathway of mechanoreceptors, which is a crucial step in the development of bone insertion devices.

3.2. Rheological response

The rheological response of the suspension revealed its non-Newtonian shear-thinning behavior. The data were fitted using the Herschel-Bulkley model, as shown in Equation (5).

$$\tau = \tau_o + ky\, e^n \cap \qquad 5$$

Where τ corresponding a shear stress (Pa), τ_o is the yield stress (Pa), k is the consistency index (Pa * s^n), γ is the shear rate (s^{-1}) and n is the flow index (dimensionless). The measured values in the suspension are presented in Table 2. The adjusted R^2 value was 0,99.

Considering the printing conditions, the inner diameter of the needle, and the volumetric flow rate of the suspension, the shear rate was calculated using Equation (6).

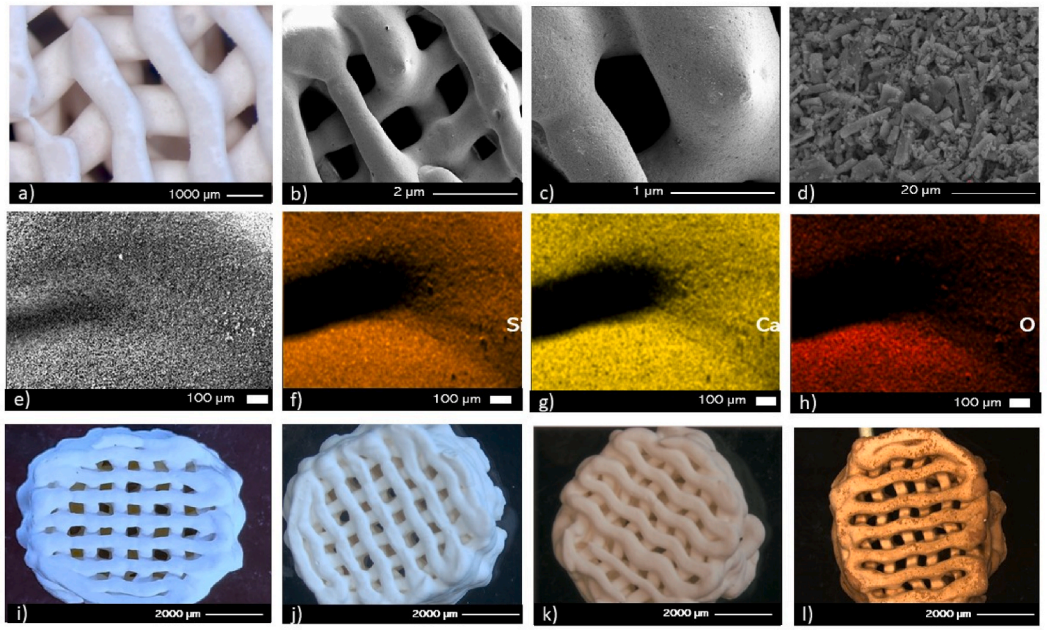

Fig. 1. SEM Scanning Electron Microscopy (SEM) images of the scaffolds obtained through 3D printing. a-b) the curvature in the printed layers can be observed, as well as the c) three-dimensional structure of the macropore walls, and finally, d-e) the prismatic structure of the characteristic wollastonite crystals. f-h) Elemental Energy-Dispersive X-ray Spectroscopy (EDS) characterization of the scaffold obtained by 3D printing, showing the presence of Si, Ca, and O. i-j) Macrophotographs of the untreated scaffolds (US) Scaffolds without propolis. k-l)Macrophotographs of the impregnated scaffolds of propolis (IS).

$$\gamma = 4Q \,/\, \pi R^3 \quad (6)$$

where $Q = 3.32x10^{-9}$ m^3/s (calculated as the volume of the printed paste divided by the time required to print that volume) is the flow rate at the needle tip, and $R = 4.19x10^{-4}$ m is the internal radius of the needle. Therefore, the shear rate (γ) of the suspensions during printing was calculated to be 57.43 s^{-1}, with an approximate viscosity of 0.155 Pa*s. When working with 3D inkjet printing, fluids are typically subjected to shear rates higher than 10^4 s^{-1} and residence times on the order of 5–250 μs [49]. However, the value reported in this study is significantly lower, which is due to the presence of particle-laden ink, whose rheological behavior can differ from that of particle-free ink [50]. The reported values are similar to those found in studies of cement materials used for 3D printing, which also exhibit a particulate composition [51].

The apparent viscosity of a fluid, which represents its resistance to flow, is defined as the shear stress divided by the shear rate [52]. It is one of the most significant variables in the analysis of the rheological behavior of inks used in 3D printing. However, in the design of inks for 3D printing, viscosity varies depending on temperature and shear stress applied during the printing process. In general, 3D printing inks should exhibit non-Newtonian behavior [53]. Flows following the Herschel-Bulkley model demonstrate non-Newtonian behavior within certain ranges of shear rate. However, outside of these ranges, a constant viscosity response is obtained, as observed in the results of this study. Such flows are characterized by their stability within these ranges, facilitating the printing processes [54].

Clay paste is one of the most referenced models in the 3D printing of ceramics [55]. It is characterized by having viscosities not exceeding 0.2 Pa*s, allowing for the attainment of high-resolution details in layer-by-layer modeling. The viscosity value obtained with the formulated Wollastonite paste in this study is very close to that of the clay paste, explaining its ability to form three-dimensional structures through 3D printing.

3.3. FTIR spectra

Fig. 2 (a and b) shows the FTIR spectra corresponding to propolis and wollastonite scaffolds impregnated with propolis. The characteristic vibrational modes of propolis are observed in the region of 3200 cm^{-1} to 3600 cm^{-1}. It is possible to observe a broad peak associated with the O–H stretching vibrational mode, which is commonly present in the phenolic groups of propolis. The presence of flavonoids can be identified as typical signals of aromatic CH2, CH, and C═C groups in the region of 1340 cm^{-1} to 1360 cm^{-1}. Primary and secondary alcohols can be identified as characteristic bands associated with C–C, C–OH, and C–C–C groups in the region of 800 cm^{-1} to 1100 cm^{-1} [30,56]. The peaks corresponding to wollastonite can be identified in the range of 400 cm^{-1} to 1200 cm^{-1}. In the region of 1010 cm^{-1} to 1100 cm^{-1}, the vibrational modes corresponding to Si–*O*–Si antisymmetric stretching vibration and O–Si–O symmetric and antisymmetric stretching vibration are found. Additionally, the peaks located at 896 cm^{-1} and 930 cm^{-1} can be associated with the non-bridging silicon-oxygen bond of Si–O, while the absorption peaks located between 450 cm^{-1} and 450 cm^{-1} are associated with the vibrational modes of Ca–O [57,58]. Table 3 summarizes the information on the main peaks identified in the FTIR spectra. These results show that the impregnation of the scaffolds using the methodology described above was successful.

3.4. Antimicrobial activity

The antimicrobial activity of ethanol extracts of propolis was measured in three different ways, and the results are shown in Fig. 3a-d. First, the Minimum Inhibitory Concentration (MIC) was obtained against *Staphylococcus aureus* (ATCC 25175) and *Staphylococcus epidermidis* (ATCC 12228). Then, inhibition zones were measured, and finally, the formation of biofilms on the scaffolds was quantified in 24 and 48-h cultures. The sensitivity of the evaluated strains to the propolis extracts was found using all three methodologies. The MIC was found to be between 1.1 ± 0.5 mg/mL against *S. aureus* and between 1.7 ± 0.3 mg/mL against *S. epidermidis*. Propolis samples from Verona, Italy, showed similar activities when evaluated against 35 strains of *S. aureus*, with inhibition observed from a concentration of 1.2 mg/mL, and against 63 strains of *S. epidermidis*. Inhibition was obtained with concentrations ranging from 1.2 to 2.5 mg/mL [59]. However, propolis from other regions such as Algeria has shown much lower MIC values, requiring a smaller amount of propolis to inhibit growth. These samples exhibited MIC values of 0.04 and 0.06 against *S. aureus* and *S. epidermidis*, respectively [60]. Given the highly variable and complex composition of propolis, it is highly likely to find samples with variable antimicrobial activity against different bacterial species.

Zone of Inhibition assays (Fig. 3b) showed a considerable effect of the propolis ethanol extracts (EEP) against strains of *S. aureus* and *S. epidermidis*, although the effect of the positive control (C+) was much greater. Scaffolds impregnated with propolis extracts (IS) exhibited inhibitory effects against both evaluated strains, although the effect was significantly lower for *S. aureus* compared to EEP. Untreated scaffolds (US) did not show any inhibitory effect. The sensitivity of *S. aureus* to EEP and impregnated scaffolds was significantly higher than that of *S. epidermidis*.

Table 2
Herschel-Bulkley fitting parameters for Wollastonite suspensions.

Parameter	Value
τ_0	167,66
k	−139,22
n	0.01

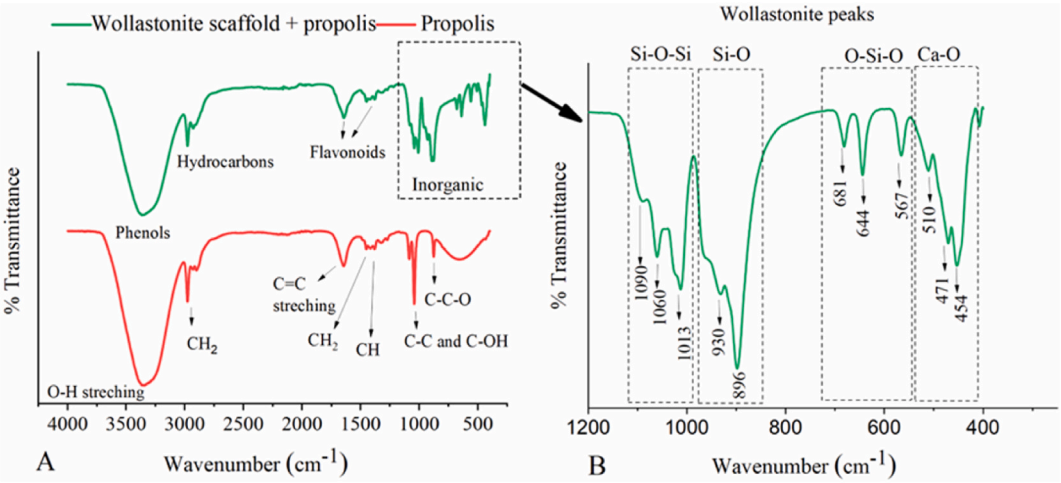

Fig. 2. FTIR analysis a) FTIR spectra of Propolis and wollastonite impregnated with propolis. b) zoom of the spectra between 400 cm^{-1} and 1200 cm^{-1}..

Table 3
Main peaks identified in the FTIR spectra of the obtained scaffolds.

Frequency cm^{-1}	Chemical Bond	Assignment
3335	O–H	OH bond
2973	C–H	Saturation CH Groups
2845	C–H	Hydrocarbons
1625	C═O	Amino acid flavonoid lipids
1647	C–O, COH	Lipid, tertiary alcohols
1513	H–O–H	Water
1453	CH, CH_2 and CH_3	Flavonoids and aromatic rings
1380	CH	CH groups of flavonoids
1269	OH C–CO	Hydrocarbons
1080	C–C, C–OH	Flavonoids and secondary alcohol groups
1043	= C–*O*–C, C–C, C–OH	Primary alcohol groups
1070–902	O–Si–O	Silica
881	C–C–*O*-	Primary and secondary alcohol groups
567–453	SiO	SiO groups
453	CaO	CaO groups

Propolis samples from different regions of Anatolia, Turkey, exhibited inhibition zones ranging from 8 to 11 mm against *S. aureus* and from 8 to 12 mm against *S. epidermidis* [61]. This kind of propolis activity has been widely reported by authors who have studied propolis from different regions, highlighting that the effect is more pronounced against gram-positive bacteria compared to gram-negative bacteria [62].

The bacterial biofilm formation assay confirmed the behavior observed in the previous tests, as significantly higher absorbance measurements were found in *S. epidermidis* cultures compared to *S. aureus* cultures, indicating that *S. aureus* is more sensitive to the effect of propolis. The IS exhibited a significant reduction in biofilm formation compared to US, and this effect persisted for up to 48 h of bacterial culture (Fig. 3d).

The antimicrobial activity of propolis has been largely attributed to the presence of organic compounds such as phenols, flavonoids, flavanones, and terpenes, among others [63,64]. The propolis used in this study showed the presence of phenolic compounds and flavonoids, indicating that these may influence the antimicrobial activity found against the evaluated species [65]. Propolis is characterized by its varied and complex composition, which allows it to affect bacterial species through mechanisms that include damage to the bacterial cell membrane [66], inhibition of bacterial enzymatic activity [67], induction of oxidative stress [68], and modulation of virulence factors [69]. Red propolis from Shandong, China has shown the ability to affect intracellular metabolite concentrations and metabolic pathways, leading to a decrease in bacterial biofilm formation, deformation of the cell wall, and reduced virulence of multidrug-resistant strains of *S. aureus* [70]. This antimicrobial effect is common among propolis from different regions and has even been observed to have antifungal activity, antimicrobial activity against mycobacteria [71], and even activity against certain viruses [72].

The activity of propolis against strains such as *S. aureus* is a significant finding, as this is one of the bacteria with a high potential to develop resistance to antibiotics including macrolides, aminoglycosides, and fluoroquinolones. This is due to the ability of these bacteria to rapidly adapt to the presence of antibiotics through their enzymatic activity [73]. Staphylococcus species are characterized

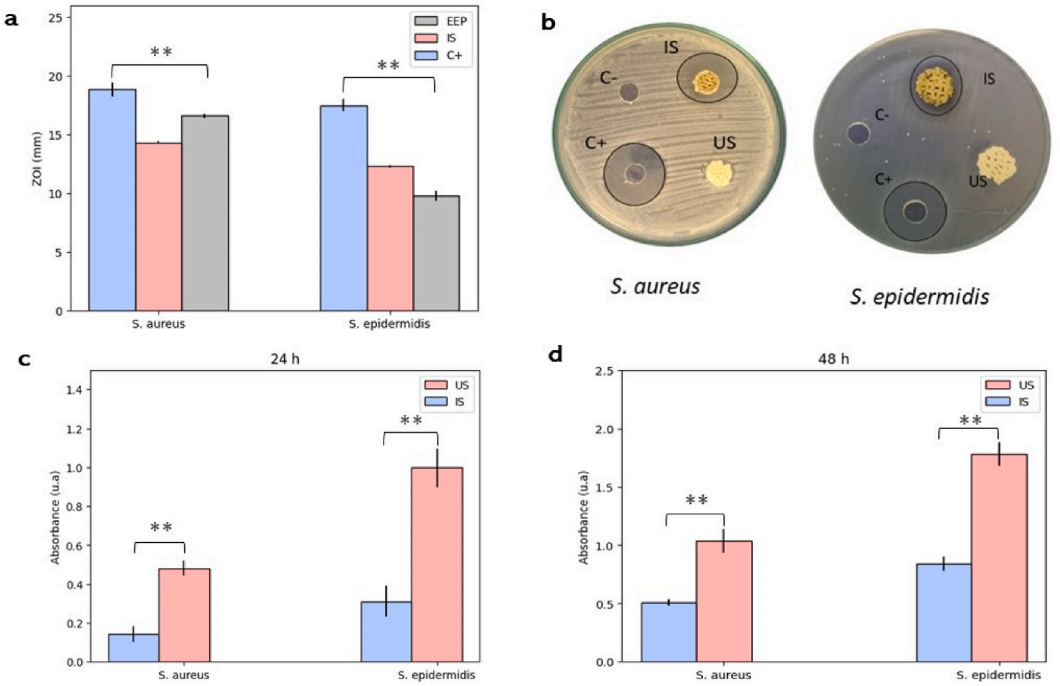

Fig. 3. Antibacterial activity. a) Zone of inhibition measurements of EEP, Untreated Scaffolds (US), and Propolis-Impregnated Scaffolds (IS) against S. aureus and S. epidermidis. b) image of inhibition zone of EEP, Untreated Scaffolds (US) and Propolis-Impregnated Scaffolds (IS) against S. aureus and S. epidermidis. c) Viability of biofilm formation after 24 h of culture on Untreated Scaffolds (US) and Propolis-Impregnated Scaffolds (IS) against S. aureus and S. epidermidis. d) Viability of biofilm formation after 48 h of culture on Untreated Scaffolds (US) and Propolis-Impregnated Scaffolds (IS) against S. aureus and S. epidermidis. Results are stated as means ± SD (n = 3) (**p ≤ 0.05, and (ns) points to non-significant difference). All the measurements of the zone of Inhibition are in mm.

by their ability to encode α-helical amphipathic peptides known as phenol-soluble modulins (PSMs) [74]. These PSMs are associated with their virulence capacity, being involved in proinflammatory and cytolytic processes, and are also related to the modulation of adhesins responsible for biofilm formation. PSMs vary among species, therefore they can exhibit different levels of sensitivity to antimicrobial agents. It is for this reason that the activity of the propolis used in this study is much higher in *S. aureus* than in *S. epidermidis*.

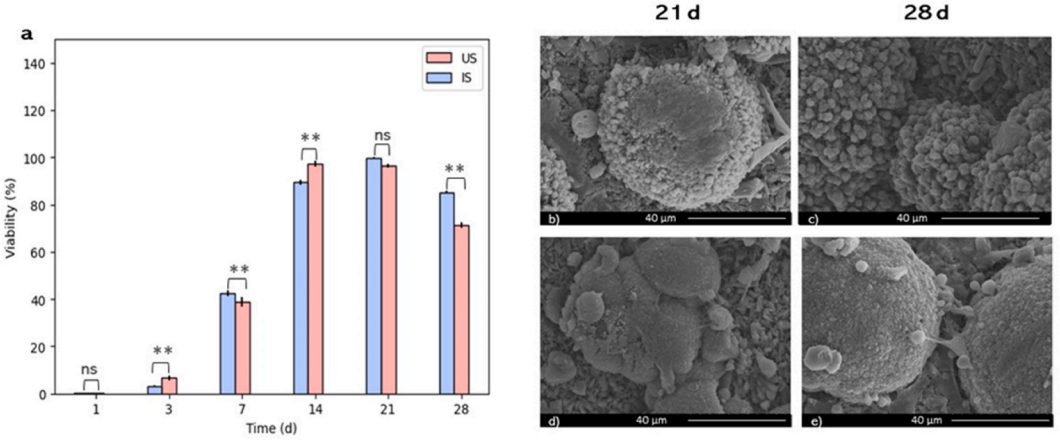

Fig. 4. Cell culture/proliferation. a) Viability Percentage of SaOS-2 on Untreated Scaffolds (US) scaffolds without propolis and Impregnated Scaffolds of propolis (IS) b) SEM of adherence of SaOS-2 on Untreated Scaffolds (US) after 21 and 28 days of culture. c-e) SEM of adherence of SaOS-2 on Impregnated Scaffolds (IS) after 21 and 28 days of culture. Results are stated as means ± SD (n = 3) (**p < 0.05, and (ns) points to non-significant difference).

3.5. Cell viability/proliferation

Cell proliferation assays showed cellular growth in both IS and US scaffolds (Fig. 4a). During the first 3 days, fluorescence signals were very low in both scaffold groups, indicating a proliferation rate of less than 10 %. From day 7 onwards, there was an increase in cell proliferation in both scaffold groups, reaching a proliferation rate of 50 %. On day 14, proliferation in both groups exceeded 80 %, showing significant differences between the two groups. In propolis-impregnated scaffolds, the proliferation process was considerably slower. This trend persisted until day 21, at which point proliferation was close to 100 % in both scaffold groups without significant differences. From day 28, a decrease in cell proliferation was observed, with a decrease of approximately 30 % compared to the proliferation achieved on day 21. SEM imaging of 21 and 28-time points (Fig. 4 b-e) revealed that the SaOs-2 cells were able to adhere, spread, and propagate on the fabricated scaffolds. SaOs-2 generally exhibited a cuboidal-like morphology typical of mature osteoblasts, and numerous filopodia interacting with other cells and the surface of scaffolds [75]. Multilayered lamellar-like structures formed by cells and presumably other extracellular matrix components were also observed [76].

The results obtained show that propolis can slow down the cell proliferation process of the SaOS-2 cell line during the first 14 days of culture. However, when proliferation reaches approximately 80 %, this effect becomes imperceptible. Propolis has been tested on human cell lines and has not shown cytotoxic effects at concentrations below 1.4 kg/mL [77]. However, when evaluated on certain types of cancer cells, including SaOS-2, it has been observed that propolis influences the processes of transporting elements into the cell, which can slow down the proliferation processes [78]. This activity has been associated with the phenolic compounds present in propolis [79], which aligns with the findings of this study, where propolis-impregnated scaffolds delayed the process of cell proliferation during the first week until reaching a cell population dense enough to survive the effect of propolis.

In addition to the effect of propolis, one of the objectives of this study was to verify if the employed three-dimensional geometry facilitates proliferative processes. This was demonstrated by achieving a viability percentage close to 100 % on day 21, indicating that the employed TPMS gyroid geometry might promote cell growth due to its interconnected porosity and the curves generated layer by layer. These results are consistent with previously reported studies, where 3D bioceramic scaffolds using materials such as bioactive glass and calcium phosphates have been shown to enhance the process of cell proliferation[80–82].

3.6. Osteogenic potential

The von Kossa staining was used as a qualitative approach to evaluate the presence of calcium-phosphate in the extracellular matrix of cell cultures (SaOs-2) or on cell/biomaterials constructs [83]. A mineralized extracellular matrix might be a reliable indicator of the osteoinductive capacity of biomaterials [84]. Fig. 5g–i shows images of cell cultures on TCPS wells, used as controls. They have been presented with positive staining for calcium-phosphate (Fig. 5h, black nodules) at day 21, and the deposition increases with the incubation time (Figs. 5i and 28 days). Both scaffold groups (Fig. 5b and c and 5e, f), showed nodules of calcium-phosphate highly distinguishable compared to control (Figure a, d). Although von Kossa is a qualitative evaluation, significant differences in intensity and area covered between both groups might be observed at 21 days. For 28 days of culture, the calcium-phosphate deposition differs in the two scaffold groups; lower area and intensity of deposits of calcium-phosphate in the extracellular matrix might be observed in

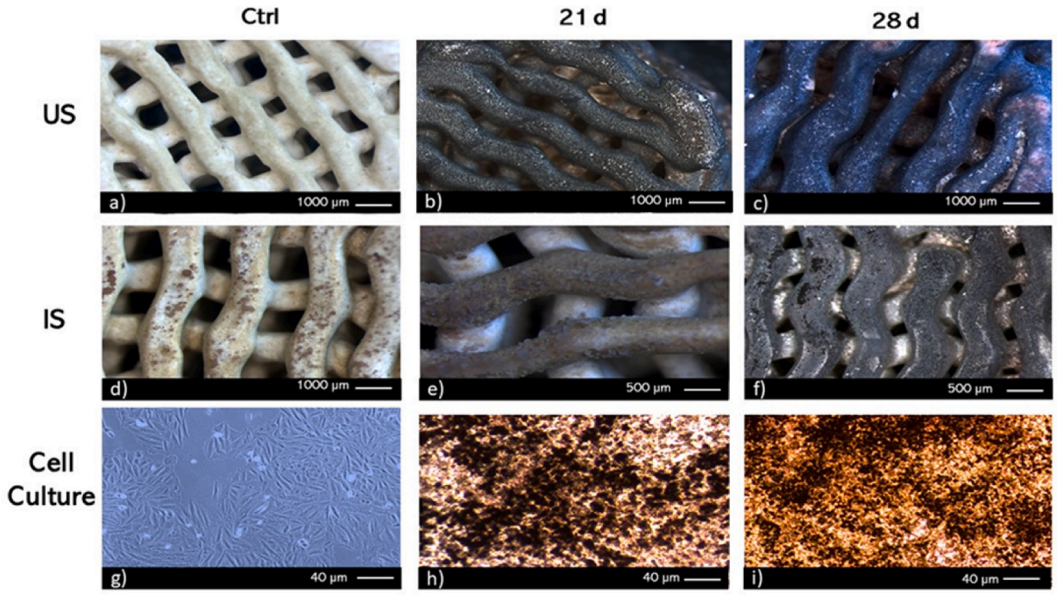

Fig. 5. von Kossa staining of SaOS-2 cultures on a-c) Untreated Scaffolds (US), d-f) Impregnated Scaffolds (IS), and g-i) TCPS. Time points. 21 and 28 days. Control (CTRL).

the IS group (Fig. 5f) compared to US group (Fig. 5c) scaffolds. These findings are consistent with previous reports [85], where positive results showed that cells exhibited a strong proliferation and osteogenic ability [86]. The areas shown are representative of the corresponding cell layer at the experimental conditions selected.

The Alizarin Red Staining was used as a qualitative approach to evaluate the presence of calcium deposits on MEC of cell cultures and constructs cells/3D-printed scaffolds. The Alizarin Red Staining for control samples revealed that no calcium deposits had been marked (Fig. 6g). Both groups of scaffolds without cells exhibit a positive staining, with little intensity (Fig. 6 a, d). After 21 days of culture, both scaffolds (Fig. 6 b, e) exhibit a marked intensity of calcium deposits, as well as, it might be observed in TCPS wells (Fig. 6h, red nodules). Finally, after 28 days of culture, all groups showed positive staining of calcium deposits (Fig. 6c, f and, i).

The alkaline phosphatase (ALP), a marker of the osteoblastic phenotype, is expressed when progenitor cells differentiate into osteoblasts. Therefore, the number of osteoblasts increases [84]. The results of the staining in the TCPS cultures, used as controls, were positive after 21 and 28 days of culture. (Fig. 7a–i). The results show that ALP was observed at both time points in this control culture, with much more intense staining on day 28. In the case of staining on the scaffolds, it can be observed that the control scaffolds exhibited a few brown colorations, while the scaffolds subjected to culture showed intense brown or black staining after 28 days (Fig. 7a,d). This staining was less marked than that used to identify calcium deposits, but it follows the same trend. After 21 days of culture (Fig. 7b, c, e,f, h), the IS group showed lower ALP staining than the US group. However, after 28 days of culture, more ALP staining can be observed in the IS group compared to the US group (Fig. 7g–i).

Histochemical (von Kossa and Alizarin Red) and ALP staining techniques qualitatively confirm that mineralization processes might be occurring on the scaffolds of both groups and that the longer they are maintained in culture, the greater the presence of ALP and calcium might be obtained. In addition, ALP staining is used to evaluate the differentiation potential of pre-osteoblastic cells to form mineralized tissues [87]. Since the assessed scaffolds increased ALP activity at longer culture times, they can be used as permanent bone substitutes since they facilitate cell proliferation and induce the formation of new bone tissue. This trend might be observed in other studies where quantitative ALP activity was evaluated where a significant and comparable increment ALP and marked von Kossa and Alizarin Red staining on the scaffolds at later time points (21 and 28 days) was found [76].

Wollastonite has the potential to be used in the development of bone replacement devices, because it favors the mineralization processes, as it has been described previously [88,89]. Wollastonite has allowed the generation of scaffolds by additive manufacturing techniques for the repair of bone defects *in vivo*, where histochemical techniques such as von Kossa and Alizarin staining have been used [90]. Wollastonite can attribute its bone regeneration-inducing properties to two important aspects, the first being its similarity to apatite in natural bone tissue, and the second to the dissolution of bioactive inorganic ions, which encourages the generation of an osteogenic environment in the pores of the scaffolds [91], where calcium and calcium-phosphate deposits might be found stained. In addition, propolis has also been used in bone repair, using chitosan as a transport medium, it was possible to demonstrate acceleration in the process of mineralization of demineralized bone matrix in its presence, this might be related to its ability to regulate the

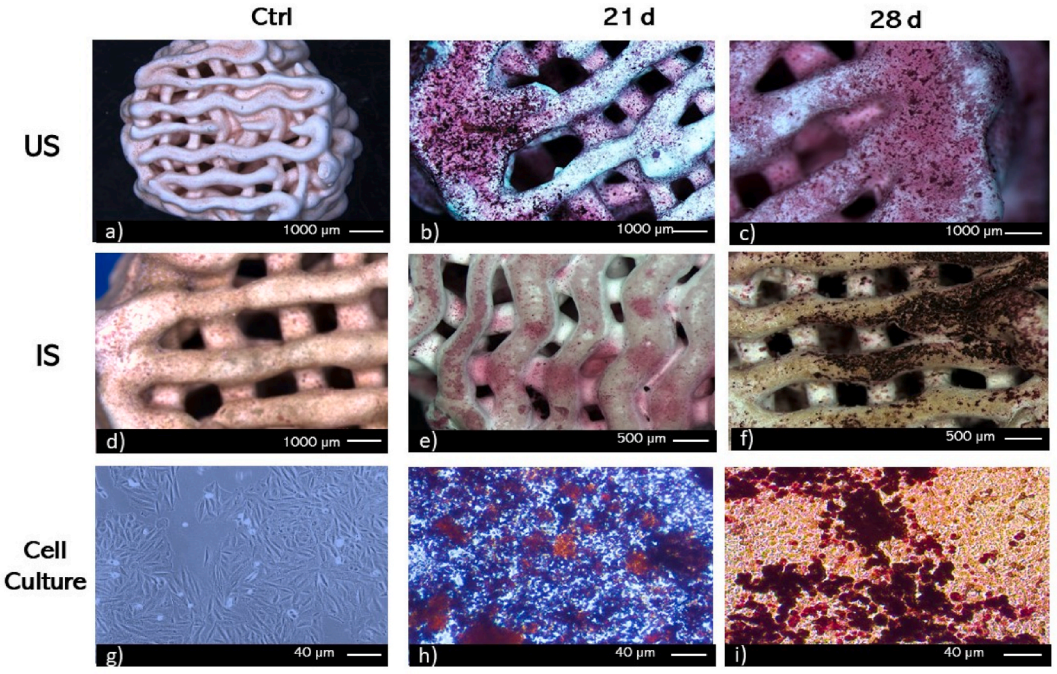

Fig. 6. Alizarin Red staining of SaOS-2 cultures on a-c) Untreated Scaffolds (US), d-f) Impregnated Scaffolds (IS) and g-i) TCPS control (CTRL). Time points. 21 and 28 days. Control (CTRL). (For interpretation of the references to color in this figure legend, the reader is referred to the Web version of this article.)

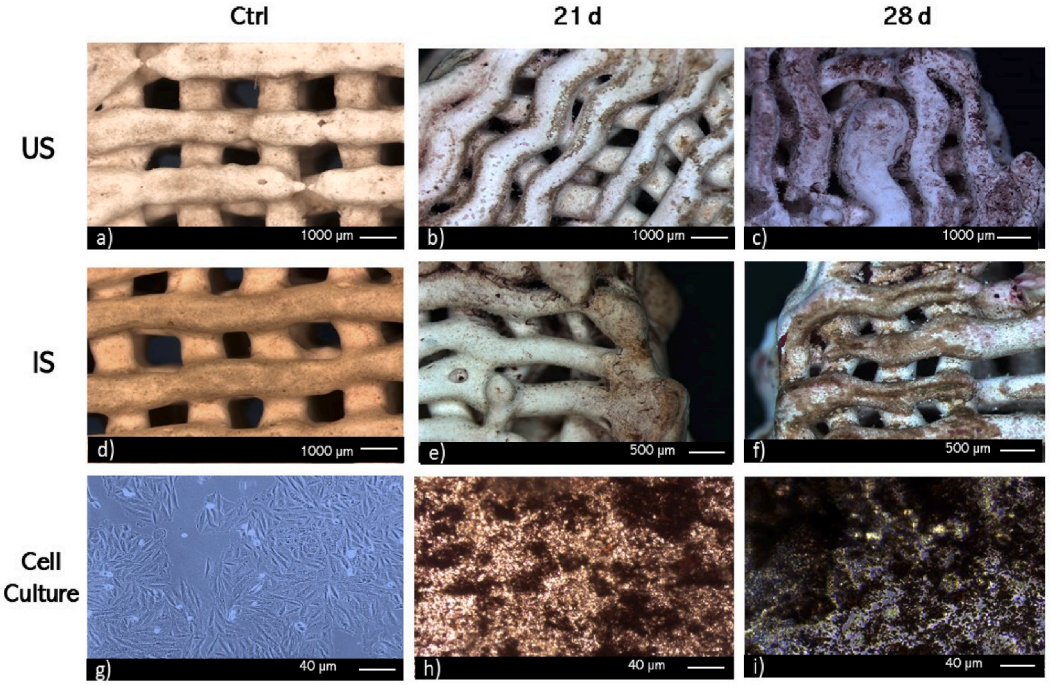

Fig. 7. ALP staining of SaOS-2 cultures on a-c) Untreated Scaffolds (US), d-f) Impregnated Scaffolds (IS), and g-i) TCPS control (CTRL). Time points. 21 and 28 days. Control (CTRL).

expression of TGF-β which is involved at earlier stages of wound healing which are conferred by the presence of some compounds such as flavonoids [92] which may be involved in inflammation modulation processes and although in this study, the inflammation process was not evaluated, it is a desirable feature when developing bone replacement devices.

3.7. Mechanical response

Fig. 8 (a and b) shows the compressive strength results of the scaffolds before and after cell proliferation tests for 21 and 28 days. Statistical analysis shows no significant differences between groups. Furthermore, the compressive strength of the scaffolds remains in the typical values measured for trabecular bone (e.g., 0.1–16 MPa) [93–95]. These results are a clear indication that the propolis impregnation treatment does not considerably affect the mechanical response and function of the scaffolds. It is worth noting in Fig. 7 that despite no statistically significant differences in the mechanical results, there is a considerable change in the variability of the results of the scaffolds after 21 and 28 days of cell proliferation in comparison to the results at 0 days. This change in the results is due to the cell proliferation and its adhesion to the scaffold, which therefore removes wollastonite particles from the surface of the scaffold in specific places, hence changing the repeatability of the results.

4. Conclusion

In this study, a ceramic paste formulation of wollastonite was successfully developed with suitable rheological characteristics for use in printing scaffolds with TPMS gyroid geometric shape, which exhibited a porosity of approximately 50 % and interconnectivity of the pores. The scaffolds were impregnated with propolis obtained from Tame, Arauca (Colombia), and their presence was confirmed through FTIR spectra analysis. The propolis impregnated in the scaffolds conferred antibacterial activity against *Staphylococcus aureus* (ATCC 25175) and *Staphylococcus epidermidis* (ATCC 12228). Inhibition zone assays and bacterial biofilm tests indicated that *S. aureus* is more sensitive to propolis's effect than *S. epidermidis*. The activity of propolis against strains like *S. aureus* is significant, as this bacterium has a high potential for developing resistance to antibiotics, including macrolides, aminoglycosides, and fluoroquinolones. The results of cell proliferation assays showed cellular growth in both propolis-impregnated (IS) and untreated (US) scaffolds. The presence of propolis in the scaffolds reduced the cell proliferation of the SaOS-2 cell line during the first 14 days of culture. However, after proliferation reached 80 %, the difference became imperceptible. The use of TPMS gyroid geometry in the scaffold design was favorable for cell proliferation. The presence of curved surfaces and interconnected porosity facilitated viability of nearly 100 % within 21 days of culture. The results obtained from von Kossa, Alizarin Red, and ALP staining assays indicate the presence of calcium and phosphorus deposits on both propolis-impregnated and un-impregnated scaffolds. The impregnation of scaffolds with propolis does not significantly affect the mechanical behavior of the scaffolds. The compressive strength of the scaffolds remains within the typical values measured for trabecular bone (e.g., 0.1–16 MPa). The results obtained in this study position propolis-impregnated wollastonite

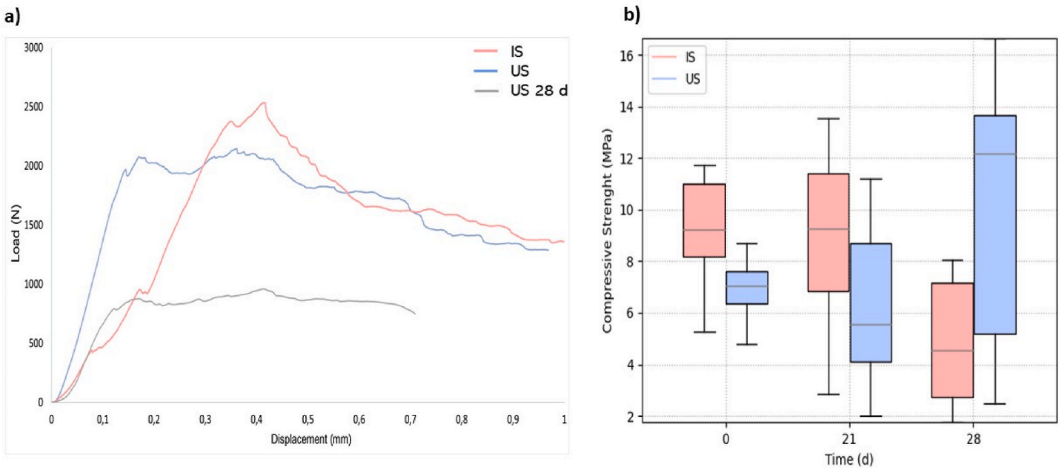

Fig. 8. Mechanical response. a) Load-displacement curve of Impregntaed scaffolds of propolis (IS) at time 0, Untreated scaffolds with propolis (US) at time 0, and Untreated scaffolds with propolis (US) at time 28 d. b) Mechanical response of 3D printed wollastonite impregnated scaffolds with propolis (IS) and Scaffolds without propolis treatment (US). There are no statistical differences between sample sets.

scaffolds as an interesting option for bone repair and regeneration.

Ethics approval and consent to participate

This study did not perform any experiments on animals. The project has the ethical endorsement of the Universidad Nacional de Colombia sede Medellín Ethics Committee, number CEMED 04419, dated August 20, 2019.

Funding statement

This work was supported by Ministerio de Ciencia Tecnologia e Innovacion Minciencias project 71203, 80740-476.2020.

Data availability statement

Data associated with this study have not been deposited into a publicly available repository, because no data was used for the research described in the article.

CRediT authorship contribution statement

Ana Isabel Moreno Florez: , Writing – original draft, Investigation. **Sarita Malagon:** Investigation. **Sebastian Ocampo:** Investigation. **Sara Leal-Marin:** Supervision, Resources, Formal analysis. **Jesús Humberto Gil González:** Resources. **Andres Diaz-Cano:** Investigation. **Alex Lopera:** Investigation. **Carlos Paucar:** Formal analysis. **Alex Ossa:** Supervision, Project administration, Investigation, Formal analysis. **Birgit Glasmacher:** Resources, Funding acquisition. **Alejandro Peláez-Vargas:** Resources, Project administration, Funding acquisition. **Claudia Garcia:** Resources, Project administration, Investigation, Funding acquisition, Formal analysis, Conceptualization.

Declaration of competing interest

The authors declare that they have no known competing financial interests or personal relationships that could have appeared to influence the work reported in this paper.

References

[1] A. Alyahya, G.R.J. Swennen, Bone grafting in orthognathic surgery: a systematic review, Int. J. Oral Maxillofac. Surg. 48 (2019) 322–331, https://doi.org/10.1016/j.ijom.2018.08.014.
[2] L. Roseti, V. Parisi, M. Petretta, C. Cavallo, G. Desando, I. Bartolotti, B. Grigolo, Scaffolds for bone tissue engineering: State of the art and new perspectives, Mater. Sci. Eng. C 78 (2017) 1246–1262, https://doi.org/10.1016/j.msec.2017.05.017.
[3] G.G. Wang, S. Deb, L.D.S. Coelho, Earthworm optimisation algorithm: a bio-inspired metaheuristic algorithm for global optimisation problems, IJBIC 12 (2018) 1, https://doi.org/10.1504/IJBIC.2018.093328.
[4] P.V. Giannoudis, H. Dinopoulos, E. Tsiridis, Bone substitutes: an update, Injury 36 (2005), https://doi.org/10.1016/j.injury.2005.07.029. S20–S27.
[5] M. Panteli, P.V. Giannoudis, Chronic osteomyelitis: what the surgeon needs to know, EFORT Open Reviews 1 (2016) 128–135, https://doi.org/10.1302/2058-5241.1.000017.

[6] K. Jerzy, H. Francis, Chronic osteomyelitis - bacterial flora, antibiotic sensitivity and treatment challenges, TOORTHJ 12 (2018) 153–163, https://doi.org/10.2174/1874325001812010153.

[7] M. Rossi, P. Marrazzo, The potential of honeybee products for biomaterial applications, Biomimetics 6 (2021) 6, https://doi.org/10.3390/biomimetics6010006.

[8] N. Martelli, C. Serrano, H. van den Brink, J. Pineau, P. Prognon, I. Borget, S. El Batti, Advantages and disadvantages of 3-dimensional printing in surgery: a systematic review, Surgery 159 (2016) 1485–1500, https://doi.org/10.1016/j.surg.2015.12.017.

[9] J. Breeze, D. Tong, A. Gibbons, Contemporary management of maxillofacial ballistic trauma, Br. J. Oral Maxillofac. Surg. 55 (2017) 661–665, https://doi.org/10.1016/j.bjoms.2017.05.001.

[10] A.L. Jardini, M.A. Larosa, R.M. Filho, C.A. de C. Zavaglia, L.F. Bernardes, C.S. Lambert, D.R. Calderoni, P. Kharmandayan, Cranial reconstruction: 3D biomodel and custom-built implant created using additive manufacturing, J. Cranio-Maxillofacial Surg. 42 (2014) 1877, https://doi.org/10.1016/j.jcms.2014.07.006, 1884.

[11] S. Bhumiratana, G. Vunjak-Novakovic, Concise review: personalized human bone grafts for reconstructing head and face, Stem Cells Translational Medicine 1 (2012) 64–69, https://doi.org/10.5966/sctm.2011-0020.

[12] H.E. Jazayeri, M. Tahriri, M. Razavi, K. Khoshroo, F. Fahimipour, E. Dashtimoghadam, L. Almeida, L. Tayebi, A current overview of materials and strategies for potential use in maxillofacial tissue regeneration, Mater. Sci. Eng. C 70 (2017) 913–929, https://doi.org/10.1016/j.msec.2016.08.055.

[13] Y. Lin, S. Huang, R. Zou, X. Gao, J. Ruan, M.D. Weir, M.A. Reynolds, W. Qin, X. Chang, H. Fu, H.H.K. Xu, Calcium phosphate cement scaffold with stem cell co-culture and prevascularization for dental and craniofacial bone tissue engineering, Dent. Mater. 35 (2019) 1031–1041, https://doi.org/10.1016/j.dental.2019.04.009.

[14] S. Hollister, C. Lin, E. Saito, C. Lin, R. Schek, J. Taboas, J. Williams, B. Partee, C. Flanagan, A. Diggs, E. Wilke, G. Van Lenthe, R. Muller, T. Wirtz, S. Das, S. Feinberg, P. Krebsbach, Engineering craniofacial scaffolds, Orthod. Craniofac. Res. 8 (2005) 162–173, https://doi.org/10.1111/j.1601-6343.2005.00329.x.

[15] F. Darus, R.M. Isa, N. Mamat, M. Jaafar, Techniques for fabrication and construction of three-dimensional bioceramic scaffolds: effect on pores size, porosity and compressive strength, Ceram. Int. 44 (2018) 18400–18407, https://doi.org/10.1016/j.ceramint.2018.07.056.

[16] R. van Noort, The future of dental devices is digital, Dent. Mater. 28 (2012) 3–12, https://doi.org/10.1016/j.dental.2011.10.014.

[17] H.N. Chia, B.M. Wu, Recent advances in 3D printing of biomaterials, J. Biol. Eng. 9 (2015) 4, https://doi.org/10.1186/s13036-015-0001-4.

[18] G.M. Azarov, E.V. Maiorova, M.A. Oborina, A.V. Belyakov, Wollastonite raw materials and their applications (a review), Glass Ceram. 52 (1995) 237–240, https://doi.org/10.1007/BF00681090.

[19] L.D. Maxim, R. Niebo, M.J. Utell, E.E. McConnell, S. LaRosa, A.M. Segrave, Wollastonite toxicity: an update, Inhal. Toxicol. 26 (2014) 95–112, https://doi.org/10.3109/08958378.2013.857372.

[20] E. Mancuso, N. Alharbi, O.A. Bretcanu, M. Marshall, M.A. Birch, A.W. McCaskie, K.W. Dalgarno, Three-dimensional printing of porous load-bearing bioceramic scaffolds, Proc. Inst. Mech. Eng. H 231 (2017) 575–585, https://doi.org/10.1177/0954411916682984.

[21] M.A. Berthaume, P.C. Dechow, J. Iriarte-Diaz, C.F. Ross, D.S. Strait, Q. Wang, I.R. Grosse, Probabilistic finite element analysis of a craniofacial finite element model, J. Theor. Biol. 300 (2012) 242–253, https://doi.org/10.1016/j.jtbi.2012.01.031.

[22] M.V. Reddy, M. Pathak, Sol-gel combustion synthesis of Ag doped CaSiO 3 : in vitro bioactivity, antibacterial activity and cytocompatibility studies for biomedical applications, Materials Technology 33 (2018) 38–47, https://doi.org/10.1080/10667857.2017.1389050.

[23] S. Palakurthy, A.A. P, V.R. K, in vitro evaluation of silver doped wollastonite synthesized from natural waste for biomedical applications, Ceram. Int. 45 (2019) 25044–25051, https://doi.org/10.1016/j.ceramint.2019.03.169.

[24] S. Azeena, N. Subhapradha, N. Selvamurugan, S. Narayan, N. Srinivasan, R. Murugesan, T. Chung, A. Moorthi, Antibacterial activity of agricultural waste derived wollastonite doped with copper for bone tissue engineering, Mater. Sci. Eng. C 71 (2017) 1156–1165, https://doi.org/10.1016/j.msec.2016.11.118.

[25] W. Ortega-Lara, D.A. Cortés-Hernández, S. Best, R. Brooks, A. Hernández-Ramírez, Antibacterial properties, in vitro bioactivity and cell proliferation of titania–wollastonite composites, Ceram. Int. 36 (2010) 513–519, https://doi.org/10.1016/j.ceramint.2009.09.024.

[26] V. Martin, I.A. Ribeiro, M.M. Alves, L. Gonçalves, R.A. Claudio, L. Grenho, M.H. Fernandes, P. Gomes, C.F. Santos, A.F. Bettencourt, Engineering a multifunctional 3D-printed PLA-collagen-minocycline-nanoHydroxyapatite scaffold with combined antimicrobial and osteogenic effects for bone regeneration, Mater. Sci. Eng. C 101 (2019) 15–26, https://doi.org/10.1016/j.msec.2019.03.056.

[27] A.S. Tiffany, D.L. Gray, T.J. Woods, K. Subedi, B.A.C. Harley, The inclusion of zinc into mineralized collagen scaffolds for craniofacial bone repair applications, Acta Biomater. 93 (2019) 86–96, https://doi.org/10.1016/j.actbio.2019.05.031.

[28] A. Sabir, A. Sumidarti, Interleukin-6 expression on inflamed rat dental pulp tissue after capped with Trigona sp. propolis from south Sulawesi, Indonesia, Saudi J. Biol. Sci. 24 (2017) 1034–1037, https://doi.org/10.1016/j.sjbs.2016.12.019.

[29] M.J.A.M. Araújo, S.D.M.G. Bosco, J.M. Sforcin, Pythium insidiosum: inhibitory effects of propolis and geopropolis on hyphal growth, Braz. J. Microbiol. 47 (2016) 863–869, https://doi.org/10.1016/j.bjm.2016.06.008.

[30] A. Del Carpio-Perochena, A. Kishen, R. Felitti, A.Y. Bhagirath, M.R. Medapati, C. Lai, R.S. Cunha, Antibacterial properties of chitosan nanoparticles and propolis associated with calcium hydroxide against Single- and multispecies biofilms: an in vitro and in Situ study, J. Endod. 43 (2017) 1332–1336, https://doi.org/10.1016/j.joen.2017.03.017.

[31] S. Duarte, P.L. Rosalen, M.F. Hayacibara, J.A. Cury, W.H. Bowen, R.E. Marquis, V.L.G. Rehder, A. Sartoratto, M. Ikegaki, H. Koo, The influence of a novel propolis on mutans streptococci biofilms and caries development in rats, Arch. Oral Biol. 51 (2006) 15–22, https://doi.org/10.1016/j.archoralbio.2005.06.002.

[32] M.F. Hayacibara, H. Koo, P.L. Rosalen, S. Duarte, E.M. Franco, W.H. Bowen, M. Ikegaki, J.A. Cury, In vitro and in vivo effects of isolated fractions of Brazilian propolis on caries development, J. Ethnopharmacol. 101 (2005) 110–115, https://doi.org/10.1016/j.jep.2005.04.001.

[33] S.A. Libério, A.L.A. Pereira, M.J.A.M. Araújo, R.P. Dutra, F.R.F. Nascimento, V. Monteiro-Neto, M.N.S. Ribeiro, A.G. Gonçalves, R.N.M. Guerra, The potential use of propolis as a cariostatic agent and its actions on mutans group streptococci, J. Ethnopharmacol. 125 (2009) 1–9, https://doi.org/10.1016/j.jep.2009.04.047.

[34] A.W. Gjertsen, K.A. Stothz, K.G. Neiva, R. Pileggi, Effect of propolis on proliferation and apoptosis of periodontal ligament fibroblasts, Oral Surgery, Oral Medicine, Oral Pathology, Oral Radiology, and Endodontology. 112 (2011) 843–848, https://doi.org/10.1016/j.tripleo.2011.08.004.

[35] M.C. Marcucci, Propolis: chemical composition, biological properties and therapeutic activity, Apidologie 26 (1995) 83–99, https://doi.org/10.1051/apido:19950202.

[36] K.B. Santiago, G.M. Piana, B.J. Conti, E.D.O. Cardoso, B.F. Murbach Teles Andrade, M.R. Zanutto, V.L. Mores Rall, A. Fernandes, J.M. Sforcin, Microbiological control and antibacterial action of a propolis-containing mouthwash and control of dental plaque in humans, Nat. Prod. Res. 32 (2018) 1441–1445, https://doi.org/10.1080/14786419.2017.1344664.

[37] I.-A.I. Thamnopoulos, G.F. Michailidis, D.J. Fletouris, A. Badeka, M.G. Kontominas, A.S. Angelidis, Inhibitory activity of propolis against Listeria monocytogenes in milk stored under refrigeration, Food Microbiol. 73 (2018) 168–176, https://doi.org/10.1016/j.fm.2018.01.021.

[38] L.A.R. Valadas, E.M. Rodrigues Neto, M.A.L. Lotif, S.G.C. Fonseca, F.O. Chagas, F.V. Fechine, C.B.M. Carvalho, M.A.M. Bandeira, M.M.F. Fonteles, P.L.D. Lobo, Evaluation of propolis dental varnish against Streptococcus mutans in children, Dent. Mater. 33 (2017), https://doi.org/10.1016/j.dental.2017.08.162 e80–e81.

[39] A. Fogden, M. Haeberlein, S. Lidin, Generalizations of the gyroid surface, J. Phys. I France. 3 (1993) 2371–2385, https://doi.org/10.1051/jp1:1993250.

[40] H. Shao, Y. He, J. Fu, D. He, X. Yang, J. Xie, C. Yao, J. Ye, S. Xu, Z. Gou, 3D printing magnesium-doped wollastonite/β-TCP bioceramics scaffolds with high strength and adjustable degradation, J. Eur. Ceram. Soc. 36 (2016) 1495–1503, https://doi.org/10.1016/j.jeurceramsoc.2016.01.010.

[41] C21 Committee, Test Method for Water Absorption, Bulk Density, Apparent Porosity, and Apparent Specific Gravity of Fired Whiteware Products, Ceramic Tiles, and Glass Tiles, ASTM International, n.d. https://doi.org/10.1520/C0373-88R06.

[42] J. Liu, X. Miao, Porous alumina ceramics prepared by slurry infiltration of expanded polystyrene beads, J. Mater. Sci. 40 (2005) 6145–6150, https://doi.org/10.1007/s10853-005-3165-3.

[43] D04 Committee, Test Method for Density of Semi-Solid Asphalt Binder (Pycnometer Method), ASTM International, n.d. https://doi.org/10.1520/D0070_D0070M-21.

[44] V. Seidel, E. Peyfoon, D.G. Watson, J. Fearnley, Comparative study of the antibacterial activity of propolis from different geographical and climatic zones: antibacterial activity of propolis from different zones, Phytother Res. 22 (2008) 1256–1263, https://doi.org/10.1002/ptr.2480.

[45] S. Leal-Marin, G. Gallaway, K. Höltje, A. Lopera-Sepulveda, B. Glasmacher, O. Gryshkov, Scaffolds with magnetic nanoparticles for tissue Stimulation, Current Directions in Biomedical Engineering 7 (2021) 460–463, https://doi.org/10.1515/cdbme-2021-2117.

[46] Peláez-Vargas, Alejandro, Daniel Gallego-Perez, D.F. Gomez, M.H. Fernandes, D.J. Hansford, F.J. Monteiro, Propagation of human bone marrow stem cells for craniofacial applications, in: M.A. Hayat (Ed.), Stem Cells and Cancer Stem Cells, 2012, pp. 107–122.

[47] S. Teixeira, M.A. Rodriguez, P. Pena, A.H. De Aza, S. De Aza, M.P. Ferraz, F.J. Monteiro, Physical characterization of hydroxyapatite porous scaffolds for tissue engineering, Mater. Sci. Eng. C 29 (2009) 1510–1514, https://doi.org/10.1016/j.msec.2008.09.052.

[48] E. Cunningham, N. Dunne, G. Walker, C. Maggs, R. Wilcox, F. Buchanan, Hydroxyapatite bone substitutes developed via replication of natural marine sponges, J. Mater. Sci. Mater. Med. 21 (2010) 2255–2261, https://doi.org/10.1007/s10856-009-3961-4.

[49] Y. Guo, H.S. Patanwala, B. Bognet, A.W.K. Ma, Inkjet and inkjet-based 3D printing: connecting fluid properties and printing performance, RPJ 23 (2017) 562–576, https://doi.org/10.1108/RPJ-05-2016-0076.

[50] P.S.R.K. Prasad, A.V. Reddy, P.K. Rajesh, P. Ponnambalam, K. Prakasan, Studies on rheology of ceramic inks and spread of ink droplets for direct ceramic ink jet printing, J. Mater. Process. Technol. 176 (2006) 222–229, https://doi.org/10.1016/j.jmatprotec.2006.04.001.

[51] R. Jayathilakage, P. Rajeev, J. Sanjayan, Rheometry for concrete 3D printing: a review and an experimental comparison, Buildings 12 (2022) 1190, https://doi.org/10.3390/buildings12081190.

[52] Mott Robert, Untener Joseph, Applied Fluid Mechanics, seventh ed., Pearson, 2014.

[53] L. Zhang, G. Yang, B.N. Johnson, X. Jia, Three-dimensional (3D) printed scaffold and material selection for bone repair, Acta Biomater. 84 (2019) 16–33, https://doi.org/10.1016/j.actbio.2018.11.039.

[54] Mary Lilliman, Control of Mortar Rheology for 3D Concrete Printing, Doctoral thesis, Loughborough University, 2017. https://hdl.handle.net/2134/25216.

[55] S.S.L. Chan, R.M. Pennings, L. Edwards, G.V. Franks, 3D printing of clay for decorative architectural applications: effect of solids volume fraction on rheology and printability, Addit. Manuf. 35 (2020), 101335, https://doi.org/10.1016/j.addma.2020.101335.

[56] Delgado, María de Lourdes, Andrade, Jesús Ángel, Ramirez, Carlos Alberto, Caracterización fisicoquímica de propóleos colectados en el Bosque La Primavera Zapopan, Jalisco., Rev. mex. de cienc. forestales. 6 (2015) 74–87.

[57] M.B. Sedelnikova, A.V. Ugodchikova, T.V. Tolkacheva, V.V. Chebodaeva, I.A. Cluklhov, M.A. Khimich, O.V. Bakina, M.I. Lerner, V.S. Egorkin, J. Schmidt, Y. P. Sharkeev, Surface modification of Mg0.8Ca alloy via wollastonite micro-arc coatings: significant improvement in corrosion resistance, Metals 11 (2021) 754, https://doi.org/10.3390/met11050754.

[58] W. Chen, Y. Liang, X. Hou, J. Zhang, H. Ding, S. Sun, H. Cao, Mechanical grinding preparation and characterization of TiO2-coated wollastonite composite pigments, Materials 11 (2018) 593, https://doi.org/10.3390/ma11040593.

[59] F. Scazzocchio, F.D. D'Auria, D. Alessandrini, F. Pantanella, Multifactorial aspects of antimicrobial activity of propolis, Microbiol. Res. 161 (2006) 327–333, https://doi.org/10.1016/j.micres.2005.12.003.

[60] S. Moussaoui, M. Lahouel, Propolis extract: a potent bacteria efflux pump inhibitor, Journal of Biologically Active Products from Nature 4 (2014) 216–223, https://doi.org/10.1080/22311866.2014.936906.

[61] A. Uzel, K. Sorkun, Ö. Önçağ, D. Çoğulu, Ö. Gençay, B. Salih, Chemical compositions and antimicrobial activities of four different Anatolian propolis samples, Microbiol. Res. 160 (2005) 189–195, https://doi.org/10.1016/j.micres.2005.01.002.

[62] U.A. Qureshi, Z. Khatri, F. Ahmed, M. Khatri, I.-S. Kim, Electrospun zein nanofiber as a green and recyclable adsorbent for the removal of reactive black 5 from the aqueous phase, ACS Sustainable Chem. Eng. 5 (2017) 4340–4351, https://doi.org/10.1021/acssuschemeng.7b00402.

[63] J. Ito, F.-R. Chang, H.-K. Wang, Y.K. Park, M. Ikegaki, N. Kilgore, K.-H. Lee, Anti-AIDS agents. 48. Anti-HIV activity of moronic acid derivatives and the new melliferone-related triterpenoid isolated from Brazilian propolis, J. Nat. Prod. 64 (2001) 1278–1281, https://doi.org/10.1021/np010211x.

[64] C.C. Duke, V.H. Tran, R.K. Duke, A. Abu-Mellal, G.T. Plunkett, D.I. King, K. Hamid, K.L. Wilson, R.L. Barrett, J.J. Bruhl, A sedge plant as the source of Kangaroo Island propolis rich in prenylated p-coumarate ester and stilbenes, Phytochemistry 134 (2017) 87–97, https://doi.org/10.1016/j.phytochem.2016.11.005.

[65] A.I. Moreno, Y. Orozco, S. Ocampo, S. Malagón, A. Ossa, A. Peláez-Vargas, C. Paucar, A. Lopera, C. Garcia, Effects of propolis impregnation on polylactic acid (PLA) scaffolds loaded with wollastonite particles against Staphylococcus aureus, Staphylococcus epidermidis, and their coculture for potential medical devices, Polymers 15 (2023) 2629, https://doi.org/10.3390/polym15122629.

[66] M.S. Almuhayawi, Propolis as a novel antibacterial agent, Saudi J. Biol. Sci. 27 (2020) 3079–3086, https://doi.org/10.1016/j.sjbs.2020.09.016.

[67] O.K. Mirzoeva, R.N. Grishanin, P.C. Calder, Antimicrobial action of propolis and some of its components: the effects on growth, membrane potential and motility of bacteria, Microbiol. Res. 152 (1997) 239–246, https://doi.org/10.1016/S0944-5013(97)80034-1.

[68] N. Vera, E. Solorzano, R. Ordoñez, L. Maldonado, E. Bedascarrasbure, M.I. Isla, Chemical composition of Argentinean propolis collected in extreme regions and its relation with antimicrobial and antioxidant activities, Nat. Prod. Commun. 6 (2011), 1934578X1100600618.

[69] R. Silva-Carvalho, F. Baltazar, C. Almeida-Aguiar, Propolis: A Complex Natural Product with a Plethora of Biological Activities that Can Be Explored for Drug Development, Evidence-Based Complementary and Alternative Medicine. 2015, 2015, pp. 1–29, https://doi.org/10.1155/2015/206439.

[70] W. Zhang, G.E. Margarita, D. Wu, W. Yuan, S. Yan, S. Qi, X. Xue, K. Wang, L. Wu, Antibacterial activity of Chinese red propolis against Staphylococcus aureus and MRSA, Molecules 27 (2022) 1693, https://doi.org/10.3390/molecules27051693.

[71] F. Saeed, R.S. Ahmad, M.U. Arshad, B. Niaz, R. Batool, R. Naz, H. Ansar Rasul Suleria, Propolis to curb lifestyle related disorders: an overview, Int. J. Food Prop. 19 (2016) 420–437, https://doi.org/10.1080/10942912.2012.745131.

[72] S. Demir, Y. Aliyazicioglu, I. Turan, S. Misir, A. Mentese, S.O. Yaman, K. Akbulut, K. Kilinc, O. Deger, Antiproliferative and proapoptotic activity of Turkish propolis on human lung cancer cell line, Nutr. Cancer 68 (2016) 165–172, https://doi.org/10.1080/01635581.2016.1115096.

[73] A. Pantosti, A. Sanchini, M. Monaco, Mechanisms of antibiotic resistance in Staphylococcus aureus, Future Microbiol. 2 (2007) 323–334.

[74] S. Periasamy, S.S. Chatterjee, G.Y.C. Cheung, M. Otto, Phenol-soluble modulins in staphylococci: what are they originally for? Commun. Integr. Biol. 5 (2012) 275–277, https://doi.org/10.4161/cib.19420.

[75] M.G. Gandolfi, F. Perut, G. Ciapetti, R. Mongiorgi, C. Prati, New portland cement–based materials for endodontics mixed with articaine solution: a study of cellular response, J. Endod. 34 (2008) 39–44, https://doi.org/10.1016/j.joen.2007.09.001.

[76] N. Higuita-Castro, D. Gallego-Perez, A. Pelaez-Vargas, F. García Quiroz, O.M. Posada, L.E. López, C.A. Sarassa, P. Agudelo-Florez, F.J. Monteiro, A.S. Litsky, D. J. Hansford, Reinforced Portland cement porous scaffolds for load-bearing bone tissue engineering applications, J. Biomed. Mater. Res. 100B (2012) 501–507, https://doi.org/10.1002/jbm.b.31976.

[77] A.H. Banskota, Y. Tezuka, S. Kadota, Recent progress in pharmacological research of propolis, Phytother Res. 15 (2001) 561–571, https://doi.org/10.1002/ptr.1029.

[78] M. Tyszka-Czochara, P. Paśko, W. Reczyński, M. Szlósarczyk, B. Bystrowska, W. Opoka, Zinc and propolis reduces cytotoxicity and proliferation in Skin fibroblast cell culture: total polyphenol content and antioxidant capacity of propolis, Biol. Trace Elem. Res. 160 (2014) 123–131, https://doi.org/10.1007/s12011-014-0019-3.

[79] A.H. Banskota, Y. Tezuka, J.K. Prasain, K. Matsushige, I. Saiki, S. Kadota, Chemical constituents of Brazilian propolis and their cytotoxic activities, J. Nat. Prod. 61 (1998) 896–900, https://doi.org/10.1021/np980028c.

[80] J. Su, S. Hua, A. Chen, P. Chen, L. Yang, X. Yuan, D. Qi, H. Zhu, C. Yan, J. Xiao, Y. Shi, Three-dimensional printing of gyroid-structured composite bioceramic scaffolds with tuneable degradability, Biomater. Adv. 133 (2022), 112595, https://doi.org/10.1016/j.msec.2021.112595.

[81] J.A. Ramírez, V. Ospina, A.A. Rozo, M.I. Viana, S. Ocampo, S. Restrepo, N.A. Vásquez, C. Paucar, C. García, Influence of geometry on cell proliferation of PLA and alumina scaffolds constructed by additive manufacturing, J. Mater. Res. 34 (2019) 3757–3765, https://doi.org/10.1557/jmr.2019.323.

[82] F. Baino, D.U. Tulyaganov, Z. Kahharov, A. Rahdar, E. Verné, Foam-replicated diopside/fluorapatite/wollastonite-based glass–ceramic scaffolds, Ceramics 5 (2022) 120–130, https://doi.org/10.3390/ceramics5010011.

[83] B. Battulga, K. Shiizaki, Y. Miura, Y. Osanai, R. Yamazaki, Y. Shinohara, Y. Kubota, T. Hara, M. Kuro-o, N. Ohno, Correlative light and electron microscopic observation of calcium phosphate particles in a mouse kidney formed under a high-phosphate diet, Sci. Rep. 13 (2023) 852, https://doi.org/10.1038/s41598-023-28103-3.

[84] Y.-C. Huang, P.-C. Hsiao, H.-J. Chai, Hydroxyapatite extracted from fish scale: effects on MG63 osteoblast-like cells, Ceram. Int. 37 (2011) 1825–1831, https://doi.org/10.1016/j.ceramint.2011.01.018.
[85] P.S. Gomes, M.H. Fernandes, Effect of therapeutic levels of doxycycline and minocycline in the proliferation and differentiation of human bone marrow osteoblastic cells, Arch. Oral Biol. 52 (2007) 251–259, https://doi.org/10.1016/j.archoralbio.2006.10.005.
[86] K. Song, Q. Kong, L. Li, Y. Wang, R. Parungao, S. Zheng, Y. Nie, Z. Jiao, H. Wang, T. Liu, fabrication and biocompatibility assay of a biomimetic osteoblastic niche, Appl. Biochem. Biotechnol. 189 (2019) 471–484, https://doi.org/10.1007/s12010-019-03015-z.
[87] H. Iqbal, M. Ali, R. Zeeshan, Z. Mutahir, F. Iqbal, M.A.H. Nawaz, L. Shahzadi, A.A. Chaudhry, M. Yar, S. Luan, A.F. Khan, I. Rehman, Chitosan/hydroxyapatite (HA)/hydroxypropylmethyl cellulose (HPMC) spongy scaffolds-synthesis and evaluation as potential alveolar bone substitutes, Colloids and Surfaces B: Biointerfaces. 160 (2017) 553–563, https://doi.org/10.1016/j.colsurfb.2017.09.059.
[88] W.E.G. Müller, E. Tolba, H.C. Schröder, B. Diehl-Seifert, T. Link, X. Wang, Biosilica-loaded poly(ϵ-caprolactone) nanofibers mats provide a morphogenetically active surface scaffold for the growth and mineralization of the osteoclast-related SaOS-2 cells, Biotechnol. J. 9 (2014) 1312–1321, https://doi.org/10.1002/biot.201400277.
[89] H.H. Lu, S.F. El-Amin, K.D. Scott, C.T. Laurencin, Three-dimensional, bioactive, biodegradable, polymer-bioactive glass composite scaffolds with improved mechanical properties support collagen synthesis and mineralization of human osteoblast-like cellsin vitro, J. Biomed. Mater. Res. 64A (2003) 465–474, https://doi.org/10.1002/jbm.a.10399.
[90] H. Shao, A. Liu, X. Ke, M. Sun, Y. He, X. Yang, J. Fu, L. Zhang, G. Yang, Y. Liu, S. Xu, Z. Gou, 3D robocasting magnesium-doped wollastonite/TCP bioceramic scaffolds with improved bone regeneration capacity in critical sized calvarial defects, J. Mater. Chem. B 5 (2017) 2941–2951, https://doi.org/10.1039/C7TB00217C.
[91] A. Liu, M. Sun, H. Shao, X. Yang, C. Ma, D. He, Q. Gao, Y. Liu, S. Yan, S. Xu, Y. He, J. Fu, Z. Gou, The outstanding mechanical response and bone regeneration capacity of robocast dilute magnesium-doped wollastonite scaffolds in critical size bone defects, J. Mater. Chem. B 4 (2016) 3945–3958, https://doi.org/10.1039/C6TB00449K.
[92] A. Meimandi-Parizi, A. Oryan, E. Sayahi, A. Bigham-Sadegh, Propolis extract a new reinforcement material in improving bone healing: an in vivo study, Int. J. Surg. 56 (2018) 94–101, https://doi.org/10.1016/j.ijsu.2018.06.006.
[93] G. Kaur, V. Kumar, F. Baino, J.C. Mauro, G. Pickrell, I. Evans, O. Bretcanu, Mechanical properties of bioactive glasses, ceramics, glass-ceramics and composites: State-of-the-art review and future challenges, Mater. Sci. Eng. C 104 (2019), 109895, https://doi.org/10.1016/j.msec.2019.109895.
[94] L. Rincón-Kohli, P.K. Zysset, Multi-axial mechanical properties of human trabecular bone, Biomech. Model. Mechanobiol. 8 (2009) 195–208, https://doi.org/10.1007/s10237-008-0128-z.
[95] L.-C. Gerhardt, A.R. Boccaccini, Bioactive glass and glass-ceramic scaffolds for bone tissue engineering, Materials 3 (2010) 3867–3910, https://doi.org/10.3390/ma3073867.